ACS APPLIED MATERIALS & INTERFACES

RESEARCH ARTICLE

www.acsami.org

Band Alignment at Organic–Inorganic Heterojunctions between P3HT and n-Type 6*H*-SiC

Roland Dietmueller,* Helmut Nesswetter, Sebastian J. Schoell, Ian D. Sharp,† and Martin Stutzmann

Walter Schottky Institut, Technische Universität München, Am Coulombwall 4, 85748 Garching, Germany

ABSTRACT: The exact band alignment at organic/inorganic semiconductor heterojunctions is influenced by a variety of properties and is difficult to predict. For organic/inorganic bilayer heterojunctions made of poly(3-hexylthiophene) (P3HT) and n-type 6*H*-SiC, the band alignment is determined via current–voltage measurements. For this purpose, a model equivalent circuit, combining thermionic emission and space-charge-limited current effects, is proposed which describes the behavior of the heterojunction very well. From the fitting parameters, an interface barrier height of 1.1 eV between the lowest unoccupied molecular orbital (LUMO) of P3HT and the conduction band (CB) of 6*H*-SiC is determined. In addition, from the maximum open circuit voltage of 6*H*-SiC/P3HT diodes, a difference of 0.9 eV between the highest occupied molecular orbital (HOMO) of P3HT and the CB of 6*H*-SiC is deduced. These two values determine the alignment of the energy bands of 6*H*-SiC relative to the HOMO and LUMO of P3HT. The 6*H*-SiC/P3HT bilayer heterojunction exhibits an open circuit voltage of ∼0.5 V at room temperature, which makes such a materials system a potential candidate for bulk heterojunction hybrid solar cells with 6*H*-SiC nanoparticles.

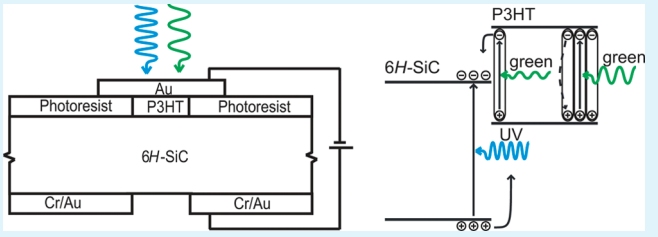

KEYWORDS: organic–inorganic heterojunction, band alignment, P3HT, silicon carbide, current–voltage measurements, type II heterojunction

INTRODUCTION

The energetic alignment at the interface of organic/inorganic heterojunctions is very important for potential hybrid solar cell and organic electronic applications. The ideal case, in which the relative position of the band edges is determined by only the Fermi levels, E_F, and the electron affinities, χ, must be adjusted due to several effects: interface dipoles at the organic/inorganic interface, which can result, for example, from chemical reactions or permanent dipoles,[1] can shift the energy levels. Furthermore, pinning of the Fermi level at surface or interface states can result in band bending.[2] Similarly, the type and level of doping of the inorganic semiconductor have a strong influence on the band alignment, as has been demonstrated with p- and n-type doping of silicon in organic/inorganic heterojunctions with silicon.[3,4]

Here, as an interesting model system for organic/inorganic heterojunctions, we choose n-type silicon carbide (SiC) as the inorganic semiconductor and the hole conductor poly(3-hexylthiophene) (P3HT) as the organic semiconductor. These materials should form a type II heterojunction from which photogenerated charge carriers can be extracted. P3HT, as a highly absorbing hole conductor, is often used in organic solar cells as the absorber, while [6,6]-phenyl-C61-butyric acid methyl ester (PCBM), which is used as the electron conductor, only absorbs in the UV region. SiC, compared to PCBM, has the advantage that it can be doped to influence the conductivity. Furthermore, by choosing different polytypes, SiC substrates with different band gaps are available.[5] SiC nanoparticles and nanowires, which are important for bulk heterojunctions, can also be produced using various methods.[6−8] Furthermore, SiC can be covalently functionalized with organic molecules[9,10] and polymers[11] in order to tune the interfacial chemical and electrical properties. For the current investigation of the alignment at the of SiC/organic semiconductor interface, we use hexagonal 6*H*-SiC with an indirect band gap of 3.0 eV[12] and P3HT with an optical band gap of 1.9 eV for two primary reasons. First, P3HT can be illuminated in the visible spectral range through the 6*H*-SiC directly at the bilayer heterojunction due to the large band gap of 6*H*-SiC. Second, literature values of the energy levels suggest that the heterojunction should allow efficient splitting of the exciton at the interface, rather than recombination or energy transfer,[13] and thus provide a reasonable V_{OC}.

This energetic alignment is shown in Figure 1a, in which the range of the literature values for the band positions of the two semiconductors is shown in gray and the continuous black lines represent the averages. Also shown in Figure 1a are the Fermi levels of n-type 6*H*-SiC and P3HT as dotted lines and the values for the work functions of the metals which were used for ohmic contacts. The expected band diagram due to Fermi level alignment of 6*H*-SiC and P3HT is shown in Figure 1b, where a space charge region in 6*H*-SiC with the corresponding band bending is present. In P3HT, which is undoped, no band bending is expected, which was confirmed by surface photovoltage measurements on P3HT under vacuum. The relative alignment of the two semiconductors is derived from the alignment of the Fermi levels of

Received: July 22, 2011
Accepted: September 21, 2011
Published: September 21, 2011

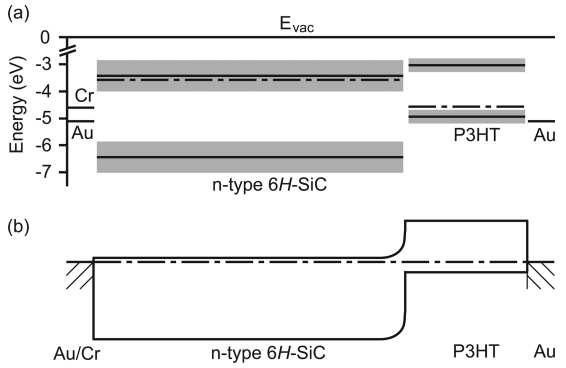

Figure 1. (a) Energy band positions of the materials used for the P3HT/6*H*-SiC heterojunction. The ranges of the literature values for 6*H*-SiC and P3HT are shown by the gray bands, whereas the continuous black lines represent the averages. The dash-dotted lines show the Fermi levels in 6*H*-SiC and P3HT. (b) Band alignment at the P3HT/6*H*-SiC heterojunction as expected from Fermi level alignment.

6*H*-SiC and P3HT. The Fermi level of 6*H*-SiC is about 120 meV below the conduction band (CB),[14] whereas in P3HT it was determined by contact potential difference measurements to be about 4.4 eV below the vacuum level which is in good agreement with the literature value of about 4.6 eV.[15] The value for the absolute position of the valence band (VB) of 6*H*-SiC was determined by Van de Walle et al.[16] and Dillon et al.[17] to be 5.9 and 6.0 eV below the vacuum level. On the other hand, our own contact potential difference measurements indicate a value of about 7 eV, which is in good agreement with the value of 6.7 eV reported by Pelletier et al.[14] For the distance of the HOMO and LUMO of P3HT to the vacuum level, literature values were used.[18−20]

In this work, we present a detailed study of 6*H*-SiC/P3HT bilayer heterojunctions. Using contact potential difference measurements, temperature-dependent current−voltage characteristics, and spectrally resolved photocurrent spectroscopy, we investigate the charge generation and transfer mechanisms and determine the band alignment at the interface. In addition, we demonstrate 6*H*-SiC/P3HT solar cell structures with an open circuit voltage of up to 0.55 V at room temperature under white light illumination with 100 mW/cm^2.

EXPERIMENTAL SECTION

The n-type 6*H*-SiC substrate (SiCrystal AG) was doped to 1×10^{18} cm^{-3} with nitrogen donors and had a resistivity of $\approx 1 \times 10^{-2}$ Ω cm. The (0001) surface of the 300 μm thick wafer was polished (NovaSiC) to an rms roughness of ≤0.3 nm and was used for formation of the heterojunctions. Unless otherwise noted, all measurements were performed using (0001) oriented Si-face SiC. A backside ohmic contact was established by the evaporation of chromium and gold, followed by annealing.[9] To avoid short-circuits through the P3HT and to define the size of the heterojunction, a photolithography step was applied. On the 6*H*-SiC, which was covered with photoresist, a 0.5 mm^2 circle was patterned. In order to provide clean and oxide-free SiC surfaces for junction formation, the samples were oxidized in an oxygen plasma and then etched in hydrofluoric acid. The P3HT (Rieke Metals, Inc.) was dissolved (2 wt %) in 1,2-dichlorobenzene and spin-coated on the previously patterned 6*H*-SiC at 1200 r.p.m., which resulted in a layer thickness of 150 ± 10 nm. The solvent was chosen due to its high boiling point, which results in a slower evaporation and therefore in a higher mobility[21] and a better morphology, as confirmed by atomic force microscopy and Fourier transform infrared spectroscopy measurements

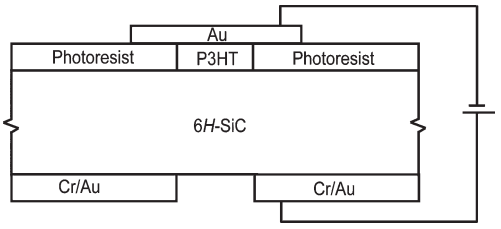

Figure 2. Schematic view of the sample structure.

on pure P3HT layers, which eliminates the need for an additional annealing step. Finally, a 7 nm thick semitransparent gold contact was evaporated as an ohmic front contact to P3HT. The transmission of the gold layer was about 50% - 70% in the relevant spectral region from 200 nm up to 600 nm. All sample preparation steps with P3HT were carried out in an argon glovebox (≤1 ppm of O_2 and H_2O). A schematic diagram of the sample structure is shown in Figure 2.

For current−voltage characteristics, which were measured under argon atmosphere, the samples were illuminated either from the 6*H*-SiC side or from the P3HT side with high-power light emitting diodes (LEDs) with wavelengths of 525 and 300 nm, and intensities of 20 and 8 mW/cm^2, respectively. Temperature-dependent and spectrally resolved measurements were performed in a nitrogen-cooled cryostat under high vacuum conditions. To exclude hysteresis effects due to trapped charges, a delay time of up to 1 s was used between the voltage steps and all current−voltage characteristics were measured cyclically. Contact potential difference measurements of SiC were performed in air directly after the etching step and for P3HT in vacuum with a gold Kelvin Probe S and a Kelvin Control 07 (Besocke Delta Phi GmbH). For surface photovoltage measurements SiC was illuminated with UV light, whereas P3HT was illuminated with white light to avoid photochemical reactions.

RESULTS AND DISCUSSION

Equivalent Circuit. For describing the current−voltage (I−V) characteristics of a solar cell, several equivalent circuits have been proposed which all include a photocurrent source, I_{Ph}, and an ideal diode. For a real solar cell, a series resistance, R_S, for ohmic losses at the contacts and in the semiconductor layers and a shunt resistance, R_{Sh}, for leakage currents are included. For steady-state measurements, which were performed in this work, the capacitance can be neglected. This results in the following I−V characteristics[2,22]

$$I = I_S\left(\exp\frac{e(V - R_S I)}{nk_B T} - 1\right) + \frac{V - R_S I}{R_{Sh}} - I_{Ph} \qquad (1)$$

where e is the elementary charge, k_B is the Boltzmann constant, T is the temperature, I_S is the reverse bias saturation current, and n is the ideality factor. This model for the I−V characteristics does not take into account any additional conduction mechanisms. In particular, the space-charge-limited current (SCLC) mechanism, which has a nonlinear current−voltage dependence, has been reported in a large variety of organic and inorganic semiconductors and solar cells.[23] The SCLC is generally described by the relationship $I = kV^m$, where m is related to the density of states of the transport path and k is related to the film thickness, trap distribution, and conductivity of the transport path. Under the assumption that the SCLC is the dominant series resistance, the ohmic term, R_S, can be neglected. Similar to the models of Pallares et al.[23] and Huynh et al.,[24] we include the SCLC transport as a nonlinear resistance, such that for a given applied voltage, V, a voltage drop at the heterojunction, V_J, and a voltage

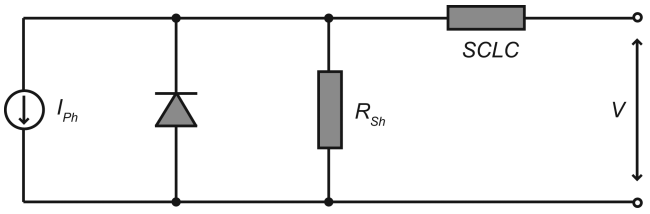

Figure 3. Equivalent circuit diagram of a solar cell, for the case in which space-charge-limited current (SCLC) effects dominate the series resistance.

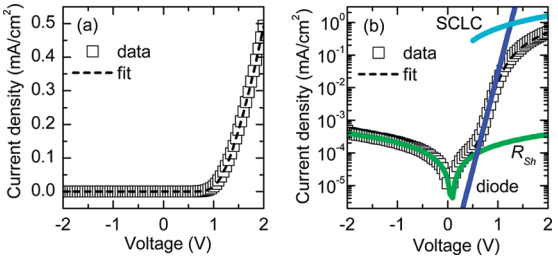

Figure 4. Dark current−voltage characteristics of the P3HT/6*H*-SiC heterojunction in (a) a linear and (b) a semilogarithmic plot. In addition to the measured data (squares), the fit (dashed line) and the individual contributions to the fit, including the shunt resistance R_{Sh} (green line), the diode (blue line), and the SCLC (cyan line), are plotted.

drop in the bulk, V_B, takes place, with $V = V_J + V_B$. The resulting equivalent circuit diagram is shown in Figure 3. For $R_{Sh} = \infty$ and without illumination, the applied voltage, V, is given by

$$V = \frac{nk_BT}{e}\ln\left(\frac{I}{I_S} + 1\right) + \left(\frac{I}{k}\right)^{1/m} \quad (2)$$

Fundamental work on organic/inorganic diodes was done by Forrest et al.,[4] who also described the $I-V$ characteristics of an organic/inorganic heterojunction as the combination of a diode at low current densities and a SCLC element at higher current densities. The diode characteristics stem from thermionic emission of majority charge carriers over a potential barrier, ϕ_{Bn}, from the doped inorganic to the undoped organic semiconductor. The thermionic emission diode[2] is described by

$$I = I_S\left[\exp\left(\frac{eV}{nk_BT}\right) - 1\right] \quad (3)$$

The reverse saturation current I_S is defined by

$$I_S = AA^*T^2\exp\left(-\frac{e\phi_{Bn}}{k_BT}\right) \quad (4)$$

when no image-force lowering of the barrier is considered and where A is the area of the diode and A^* is the effective Richardson constant, which is 194.6 A/(cm^2 K^2) for n-type 6*H*-SiC.[25]

Fit of the Dark Current−Voltage Characteristics. In Figure 4, the dark $I-V$ curve (squares) of the 6*H*-SiC/P3HT heterojunction is shown in linear and semilogarithmic plots, including the fit (dashed line) and the individual components of the fit. The positive voltage corresponds to a positive potential on the P3HT side of the junction. The symmetric shape of the $I-V$ characteristic in the semilogarithmic plot (Figure 4b) at small voltages is a strong indication for a shunt resistance R_{Sh}, which governs the reverse current of the diode. This can be fitted by R_{Sh} = 5.2 kΩ cm^2, and is shown as the green line in Figure 4b. With this value of R_{Sh}, the $I-V$ curve was then fitted using the proposed model of a series connection between the diode and the SCLC element. The overall fit, given by the dashed line in Figure 4, is in very good agreement with the data.

The extracted diode parameters, which describe the forward direction in the voltage range of 0.6 - 0.9 V, before the SCLC dominates at higher voltages, are the ideality factor n = 2.9 and the saturation current density $J_S = I_S/A = 3.5 \times 10^{-8}$ mA/cm^2. Using eq 4, a barrier height in the forward direction of $e\phi_{Bn}$ = 1.1 eV can be extracted from the saturation current. The forward direction is defined by the injection of electrons from the conduction band of 6*H*-SiC, where most of the donors are ionized at room temperature,[26] into the lowest unoccupied molecular orbital (LUMO) of the P3HT. Since the P3HT is undoped, injection of holes into the VB of 6*H*-SiC should be negligible. The calculated barrier is therefore the barrier for thermionic emission of electrons from 6*H*-SiC to the LUMO of P3HT. In the reverse direction, electrons are injected from the ohmic Au contact, which is energetically aligned with the highest occupied molecular orbital (HOMO) of P3HT, into the LUMO of P3HT. The electrons must overcome a barrier of about 1.9 eV, though this value could be reduced by the presence of surface defect states. Therefore the forward and the reverse directions of the diode are governed by different barriers at different interfaces, in contrast to standard thermionic emission diodes. Furthermore, a high defect density, leading to strong recombination at the heterojunction interface, is indicated by the large ideality factor.[27] The values for the SCLC extracted from the fit of the dark $I-V$ characteristics, are m = 1.3 and k = 0.7 mA/cm^2 V$^{1.3}$. Because of the series connection, the current through the diode and the SCLC resistance is the same, but the voltage is divided over both elements. This means, for example, that at a voltage of 0.5 V, about 0.35 V drop at the diode and about 0.15 V drop at the SCLC resistance in the P3HT. In Figure 4b, the different contributions of the SCLC (cyan line) and the diode (blue line) for the fit are also shown, under the assumption that the entire voltage drops either at the SCLC or at the diode.

Two different faces of the 6*H*-SiC sample, the Si face and the C face, were used for P3HT/SiC heterojunctions, but no significant effect on the $I-V$ characteristics was observed. This is in accordance with the contact potential difference measurements in which the difference between the two polarities was determined to be about 100 meV. Compared to the determined barrier height of 1.1 eV, the influence of the crystal polarity can be neglected.

Current−Voltage Characteristics under Illumination with Different Wavelengths. To reveal the charge generation and separation mechanisms at the heterojunction under optical excitation, the $I-V$ characteristics were measured under illumination by LEDs with center wavelengths of λ = 525 nm and λ = 300 nm from either the 6*H*-SiC side or the P3HT side. These wavelengths were chosen based on the absorption characteristics of P3HT and 6*H*-SiC. P3HT has an absorption onset at 650 nm and has an absorption maximum at about 550 nm, while 6*H*-SiC has an indirect bandgap of 3.0 eV and a corresponding absorption edge at about 400 nm with strong absorption at 300 nm. This can bee seen in the absorption spectra in Figure 5, in which the P3HT spectrum was measured and the SiC spectrum was taken from the literature.[28]

If the sample is illuminated from the P3HT side of the junction, both wavelengths generate a photocurrent I_{Ph} and a V_{OC} of up to ≈0.5 V, as shown in Figure 6a. In contrast, the $I-V$ characteristics

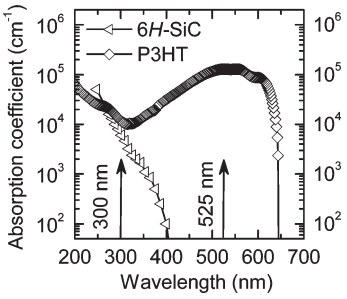

Figure 5. Absorption spectra of 6*H*-SiC (triangles) and P3HT (squares). The arrows indicate the center wavelengths of the LEDs. Data for the 6*H*-SiC are taken from ref 28.

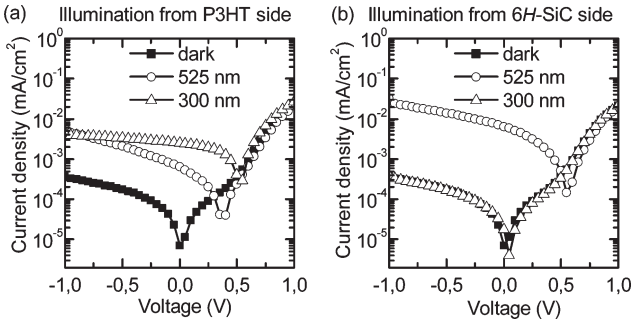

Figure 6. $I-V$ characteristics of the P3HT/6*H*-SiC heterojunction in the dark (squares) and under illumination with λ = 525 nm (circles) and λ = 300 nm (triangles) from the (a) P3HT and (b) 6*H*-SiC side of the heterojunction.

under illumination from the 6*H*-SiC side (Figure 6b) reveal a photoresponse only for λ = 525 nm. The last fact can be explained by the high absorption coefficient of $\alpha = 6.6 \times 10^3$ cm^{-1} for 6*H*-SiC at 300 nm, which leads to the absorption of all photons before they reach the interface. Because of the short diffusion length for holes of approximately 1−4 μm in 6*H*-SiC,[29] all photoexcited charge carriers recombine before reaching the heterojunction. In contrast, under UV illumination from the P3HT side, photons reach 6*H*-SiC at the heterojunction interface, as P3HT has an absorption minimum at 300 nm (Figure 5). Thus, photons are absorbed in 6*H*-SiC near the heterojunction interface and, hence, contribute to the photocurrent. The higher I_{Ph} and V_{OC} under green illumination from the 6*H*-SiC side, compared to illumination from the P3HT side, can be understood by the fact that more photons reach the interface, since 6*H*-SiC, in contrast to P3HT, does not absorb at this wavelength. Photons absorbed in the bulk P3HT do not contribute to the photocurrent because excitons in conjugated polymers have a binding energy of ~0.2 eV[30] and a diffusion length of only a few nanometers.[31] Thus, they can only be dissociated at the organic/inorganic interface.

The strong reverse bias dependence of the photocurrent under green illumination on the electric field can be explained by the fact that the charge carriers from the P3HT, even after exciton dissociation, are still bound by Coulomb attraction and can be dissociated by the electric field.[32] Furthermore, it should be mentioned that the large open circuit voltage of ~0.5 V, which was measured for both LEDs when the sample was illuminated from the P3HT side, is a promising value which makes this materials system an interesting candidate for the application in high interfacial area solar cells.

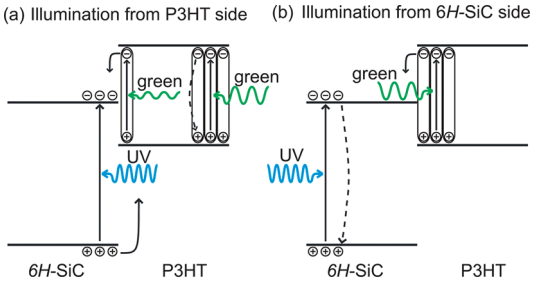

Figure 7. Schematic representation of absorption, exciton generation and dissociation, charge generation and transfer, and recombination processes under illumination with different wavelengths from (a) the P3HT and (b) the 6*H*-SiC side of the heterojunction.

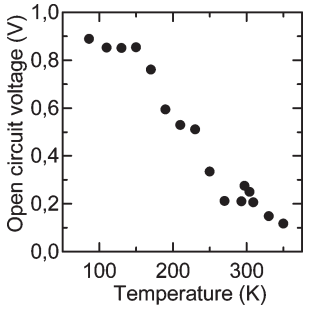

Figure 8. Values of the open circuit voltage at different temperatures. At low temperatures, a saturation is observed at a value of ~0.9 V.

The above-described processes are shown schematically in Figure 7. Photon absorption, followed by exciton and charge carrier generation in the P3HT and 6*H*-SiC, respectively, is illustrated by vertical straight arrows. The exciton dissociation at the 6*H*-SiC/P3HT interface and the charge carrier transfer from the 6*H*-SiC are indicated by curved arrows, while the recombination of charge carriers is represented by dashed arrows.

Band Alignment. To obtain more detailed information about the band alignment at the 6*H*-SiC/P3HT interface, the measurement of V_{OC} as a function of temperature under constant illumination by a Xenon lamp was performed. The V_{OC} increases with decreasing temperature and finally saturates at a value of ≈0.9 V, as shown in Figure 8. This behavior is also observed in organic solar cells, in which V_{OC} saturates with decreasing temperature at the maximum open circuit voltage V_{OC}^{max}.[33,34] Similarly, the saturation value of 0.9 V can be identified as the V_{OC}^{max} of the P3HT/6*H*-SiC heterojunction. The V_{OC}^{max} in organic solar cells is defined as the difference between the HOMO of the donor and the LUMO of the acceptor of an organic heterojunction minus a typical offset of approximately 0.3 eV due to the binding energy of the intermediate geminate polaron pair, as observed at pure organic donor−acceptor interfaces.[34,35] However, at the hybrid P3HT/6*H*-SiC interface, we can neglect such an offset and adapt the definition of V_{OC}^{max} to our system as follows

$$eV_{OC}^{max} = E_{HOMO}^{P3HT} - E_{CB}^{6H-SiC} \quad (5)$$

where $E_{CB}^{6H\text{-}SiC}$ and E_{HOMO}^{P3HT} are the energy positions of the CB of 6*H*-SiC and of the HOMO of P3HT relative to vacuum, respectively. Therefore, one can deduce from V_{OC}^{max} that the energy difference between the HOMO of P3HT and the CB of 6*H*-SiC is 0.9 eV.

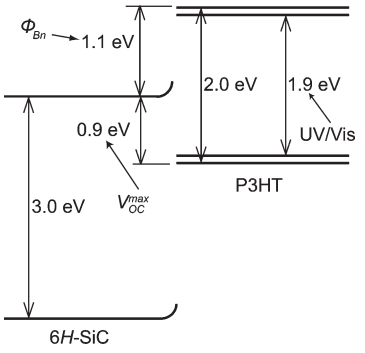

Figure 9. Experimentally determined band alignment at the P3HT/6*H*-SiC heterojunction.

By adding this value to the value of $e\phi_{Bn}$ = 1.1 eV, the bandgap of P3HT is obtained with eV_{OC}^{max} + $e\phi_{Bn}$ = 2.0 eV. The optical bandgap of P3HT was measured via absorption spectroscopy to be approximately 1.9 eV. This value is in excellent agreement with the value of 2.0 eV determined here, since the exciton binding energy for polymers of about 0.2 eV[30] must be added to the value of the optical band gap to obtain the transport band gap. Thus, the values of V_{OC}^{max} and ϕ_{Bn}, which both independently define the relative alignment of the energy bands, are consistent within the experimental accuracy. The determined alignment of the 6*H*-SiC and the P3HT energy levels, as shown in Figure 9, is within the range of the literature values, shown in Figure 1a, which were used for prediction of the interface energetics. When using our experimental values for the work function of 6*H*-SiC, which were obtained by contact potential difference measurements, and the average literature values of the P3HT, a remarkably good agreement between the predicted and the measured band alignment is achieved.

With the V_{OC}^{max} of 0.9 V and the ϕ_{Bn} of 1.1 V, the position of the conduction band minimum of 6*H*-SiC relative to the LUMO and the HOMO of P3HT is determined. Furthermore, for bulk 6*H*-SiC the energy difference between the Fermi level and the conduction band minimum is well-defined. However, directly at the interface, we only know the total barrier height, ϕ_{Bn}, which may consist of two contributions: a depletion region in the 6*H*-SiC and the offset between the CB of 6*H*-SiC and the LUMO of P3HT. To clarify the different contributions and hence the exact band alignment at the interface of P3HT and 6*H*-SiC, were performed surface photovoltage measurements of the freshly etched 6*H*-SiC surface and an upward band bending of 0.3 - 0.4 eV was measured. This band bending at the surface of 6*H*-SiC was attributed to Fermi level pinning at surface defect states. When a further charge transfer between the 6*H*-SiC and the P3HT is neglected, this can be a rough estimate of the depletion layer in the 6*H*-SiC at the heterojunction interface. However, additional measurements will be required to specifically determine the interfacial band bending following junction formation.

CONCLUSION

In this paper, the heterojunction between n-type 6*H*-SiC and undoped P3HT was investigated. An equivalent circuit was proposed, which includes a diode, a SCLC element, and a shunt resistance. The *I*−*V* characteristics of the organic/inorganic heterojunction P3HT/6*H*-SiC could be described by thermionic emission of electrons from the conduction band of the n-type 6*H*-SiC over a barrier into the LUMO of P3HT. From the diode fitting parameters, this barrier was determined to be ϕ_{Bn} = 1.1 V. This value is in excellent agreement with the offset of 0.9 V between the CB of 6*H*-SiC and the HOMO of P3HT, which was determined from temperature-dependent measurements of the open circuit voltage under illumination. Light-induced charge generation and separation processes in the different materials were investigated via selective excitation from the P3HT or 6*H*-SiC side, respectively. Due to the small exciton diffusion length in P3HT and the low hole mobility in 6*H*-SiC, only the photons that are absorbed near the heterojunction contribute to the photocurrent. However, a significant open circuit voltage of ~0.5 V was achieved. This suggests that a hybrid bulk heterojunction solar cell with 6H-SiC nanoparticles and P3HT may be interesting for photovoltaic applications due to the enhanced interfacial area.

AUTHOR INFORMATION

Corresponding Author

*E-mail: dietmueller@wsi.tum.de.

Current Address

†Joint Center for Artificial Photosynthesis, Lawrence Berkeley National Laboratory, 1 Cyclotron Rd., Berkeley, CA 94720.

ACKNOWLEDGMENT

S.J.S. and I.D.S. acknowledge the financial support of the Technische Universität München−Institute for Advanced Study, funded by the German Excellence Initiative.

REFERENCES

(1) Ishii, H.; Sugiyama, K.; Ito, E.; Seki, K. *Adv. Mater.* **1999**, *11*, 605–625.

(2) Sze, S.; Ng, K. *Physics of Semiconductor Devices*; John Wiley & Sons: Hoboken, NJ, 2007.

(3) Niesar, S.; Dietmueller, R.; Nesswetter, H.; Wiggers, H.; Stutzmann, M. *Phys. Status Solidi (a)* **2009**, *206*, 2775–2781.

(4) Forrest, S. R.; Kaplan, M. L.; Schmidt, P. H. *J. Appl. Phys.* **1984**, *55*, 1492.

(5) Fisher, G. R.; Barnes, P. *Philos. Mag. B* **1990**, *61*, 217.

(6) Shen, G.; Chen, D.; Tang, K.; Qian, Y.; Zhang, S. *Chem. Phys. Lett.* **2003**, *375*, 177–184.

(7) Honda, S.-I.; Baek, Y.-G.; Ikuno, T.; Kohara, H.; Katayama, M.; Oura, K.; Hirao, T. *Appl. Surf. Sci.* **2003**, *212*−*213*, 378–382.

(8) Liu, Z.; Ci, L.; Jin-Phillipp, N. Y.; Ruehle, M. *J. Phys. Chem. C* **2007**, *111*, 12517–12521.

(9) Schoell, S. J.; Hoeb, M.; Sharp, I. D.; Steins, W.; Eickhoff, M.; Stutzmann, M.; Brandt, M. S. *Appl. Phys. Lett.* **2008**, *92*, 153301.

(10) Rosso, M.; Giesbers, M.; Arafat, A.; Schroen, K.; Zuilhof, H. *Langmuir* **2009**, *25*, 2172–2180.

(11) Steenackers, M.; Sharp, I. D.; Larsson, K.; Hutter, N. A.; Stutzmann, M.; Jordan, R. *Chem. Mater.* **2010**, *22*, 272–278.

(12) Levinshtein, M.; Rumyantsev, S.; Shur, M. *Properties of Advanced Semiconductor Materials: GaN, AlN, InN, BN, SiC, SiGe*; John Wiley & Sons: New York, 2001.

(13) Gowrishankar, V.; Scully, S. R.; McGehee, M. D.; Wang, Q.; Branz, H. M. *Appl. Phys. Lett.* **2006**, *89*, 252102.

(14) Pelletier, J.; Gervais, D.; Pomot, C. *J. Appl. Phys.* **1984**, *55*, 994.

(15) Cascio, A. J.; Lyon, J. E.; Beerbom, M. M.; Schlaf, R.; Zhu, Y.; Jenekhe, S. A. *Appl. Phys. Lett.* **2006**, *88*, 062104.

(16) Van de Walle, C. G.; Neugebauer, J. *Nature* **2003**, *423*, 626–628.

(17) Dillon, J. A.; Schlier, R. E.; Farnsworth, H. E. *J. Appl. Phys.* **1959**, *30*, 675.
(18) Chirvase, D.; Chiguvare, Z.; Knipper, M.; Parisi, J.; Dyakonov, V.; Hummelen, J. C. *Synth. Met.* **2003**, *138*, 299–304.
(19) Oku, T.; Nagaoka, S.; Suzuki, A.; Kikuchi, K.; Hayashi, Y.; Inukai, H.; Sakuragi, H.; Soga, T. *J. Phys. Chem. Solids* **2008**, *69*, 1276–1279.
(20) Thakur, A. K.; Mukherjee, A. K.; Preethichandra, D. M. G.; Takashima, W.; Kaneto, K. *J. Appl. Phys.* **2007**, *101*, 104508.
(21) Chang, J.-F.; Sun, B.; Breiby, D. W.; Nielsen, M. M.; Soelling, T. I.; Giles, M.; McCulloch, I.; Sirringhaus, H. *Chem. Mater.* **2004**, *16*, 4772–4776.
(22) Wuerfel, P. *Physik der Solarzellen*; Spektrum Akademischer Verlag: Heidelberg, Berlin, 2000.
(23) Pallarees, J.; Cabree, R.; Marsal, L. F.; Schropp, R. E. I. *J. Appl. Phys.* **2006**, *100*, 084513.
(24) Huynh, W. U.; Dittmer, J. J.; Teclemariam, N.; Milliron, D. J.; Alivisatos, A. P.; Barnham, K. W. J. *Phys. Rev. B* **2003**, *67*, 115326.
(25) Reshanov, S. A.; Emtsev, K. V.; Speck, F.; Gao, K.; Seyller, T. K.; Pensl, G.; Ley, L. *Phys. Status Solidi (b)* **2008**, *245*, 1369–1377.
(26) Ruff, M.; Mitlehner, H.; Helbig, R. *IEEE Trans. Electron Devices* **1994**, *41*, 1040–1054.
(27) Breitenstein, O.; Bauer, J.; Lotnyk, A.; Wagner, J. *Superlatt. Microstr.* **2009**, *45*, 182–189.
(28) Philipp, H.; Taft, E. *Silicon Carbide—A High Temperature Semiconductor*; Pergamon Press: Oxford, U.K., 1960.
(29) Polyakov, A. Y.; Li, Q.; Huh, S. W.; Skowronski, M.; Lopatiuk, O.; Chernyak, L.; Sanchez, E. *J. Appl. Phys.* **2005**, *97*, 053703.
(30) Campbell, I. H.; Hagler, T. W.; Smith, D. L.; Ferraris, J. P. *Phys. Rev. Lett.* **1996**, *76*, 1900.
(31) Markov, D. E.; Amsterdam, E.; Blom, P. W. M.; Sieval, A. B.; Hummelen, J. C. *J. Phys. Chem. A* **2005**, *109*, 5266–5274.
(32) Deibel, C.; Strobel, T.; Dyakonov, V. *Phys. Rev. Lett.* **2009**, *103*, 036402.
(33) Riedel, I.; Parisi, J.; Dyakonov, V.; Lutsen, L.; Vanderzande, D.; Hummelen, J. C. *Adv. Funct. Mater.* **2004**, *14*, 38–44.
(34) Rand, B. P.; Burk, D. P.; Forrest, S. R. *Phys. Rev. B* **2007**, *75*, 115327.
(35) Brabec, C. J.; Cravino, A.; Meissner, D.; Sariciftci, N. S.; Fromherz, T.; Rispens, M. T.; Sanchez, L.; Hummelen, J. C. *Adv. Funct. Mater.* **2001**, *11*, 374–380.